A new interpretation of large amplitude earthquake acceleration from non-linear local soil-structure interaction

Kotaro KOJIMA[1], Shuichi KAMAGATA[2] and Izuru TAKEWAKI[1*]

[1] *Dept. of Architecture and Architectural Eng., Kyoto University, Kyoto 615-8540, Japan*

[2] *Nuclear Power Department, Kajima Corporation, Tokyo 107-8348, Japan*

**Corresponding author: takewaki@archi.kyoto-u.ac.jp*

Abstract

A new interpretation of large amplitude earthquake accelerations recorded at the Kashiwazaki-Kariwa nuclear power station during the Niigata-ken Chuetsu-oki earthquake in 2007 is provided from the viewpoint of non-linear local interaction between an embedded building and its surrounding soil. An occurrence mechanism is investigated by the dynamic response analysis in which a bi-linear restoring-force characteristic with a gap-slip process is used. The Ricker wavelet and the continuous sweep sinusoidal wave are adopted as an input. The amplification is explained to be induced by an additional higher mode due to the change of a support condition, such as a gap between an embedded building and its surrounding soil.

Keyword ; large amplitude acceleration, support condition, non-linear interaction, embedded building, surrounding soil, gap-slip process, Ricker wavelet, continuous sweep sinusoidal wave, non-stationary Fourier spectra, nuclear power station

1. Introduction

Three earthquakes, Niigata-ken Chuetsu-oki earthquake in 2007, Suruga-bay earthquake in 2009 and the 2011 off the Pacific coast of Tohoku earthquake, stopped the operation of nuclear power stations located near each epicenter (see Fig.1). At the sacrifice of high seismic hazard, many precious seismic records were obtained, since a high density array of seismometers had been arranged in each nuclear power station.

Since the maximum acceleration 6.8m/s^2 at the foundation of the No.1 unit reactor building exceeded the maximum design value 2.7 m/s^2, the re-examination of seismic design force was started after the Niigata-ken Chuetsu-oki earthquake in 2007 (Nuclear Safety Commission of Japan, 2012, Japan Nuclear Energy Safety Organization, 2008, 2009a). The authors analyzed the seismic records and investigated the occurrence

mechanism of the large acceleration value (Kamagata and Takewaki, 2013a). One of the authors participated in the field investigation of the Kashiwazaki-Kariwa nuclear station one month after the earthquake and paid attention to the non-linear behavior between the embedded building and the surrounding soil (Kamagata, 2009, Japan Nuclear Energy Safety Organization, 2009b).

Two years after the above-mentioned earthquake, the maximum acceleration 4.38m/s^2 was measured at the Hamaoka nuclear power station during the Suruga-bay earthquake in 2009. The authors analyzed the seismic records and detected a local vibration mode in the underground soil beneath the building and the rocking behavior of building foundation by the numerical integrated displacement profiles (Kamagata and Takewaki, 2013b).

During the 2011 off the Pacific coast of Tohoku earthquake, the operation of Fukushima Daiichi nuclear power station was automatically stopped and the tsunami after the earthquake caused the blackout of the station, which stopped the cooling system and caused the meltdown of the nuclear reactor, the hydrogen explosion and the radioactive contamination. The authors analyzed the seismic records at the Onagawa nuclear power station and have found that the level of measured seismic records was almost equivalent to the extreme design basis earthquake (Kamagata and Takewaki, 2013c).

Fig.1 Epicenter of three earthquakes (Niigata-ken Chuetsu-oki earthquake in 2007, Suruga-bay earthquake in 2009, the 2011 off the Pacific coast of Tohoku earthquake) and location of nuclear power stations (http://www5.ocn.ne.jp/~botan/map_g.html)

The typical seismic records during these three seismic events are compared in Fig.2, in which the acceleration 6.8m/s^2 in the EW component at the foundation of the reactor building No.1 unit during Niigata-ken Chuetsu-oki earthquake in 2007 (designated as 1R2(EW)) is the largest among three records.

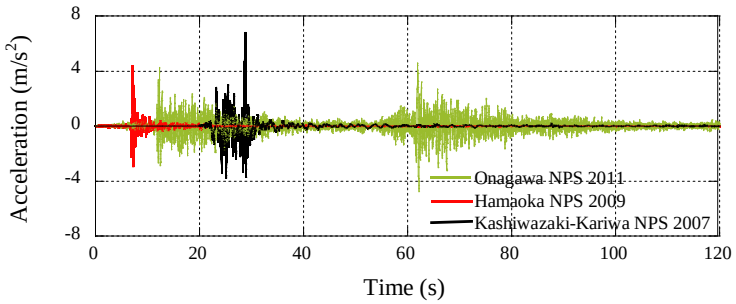

Fig.2 Comparison of ground motions of three seismic events

Table 1 Specification of seismic records (m/s^2)

	Earthquake magnitude	Focal depth (km)	Epicentral distance (km)	PGA (m/s^2)
Onagawa NPS 2011	M9.0	24	123	4.20
Hamaoka NPS 2009	M6.5	23	37	4.38
Kashiwazaki-Kariwa NPS 2007	M7.2	17	15	6.8

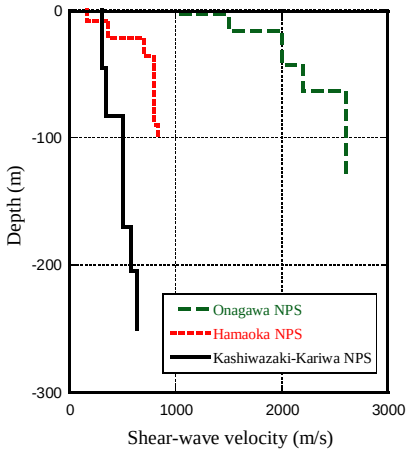

Fig.3 Comparison of shear-wave velocity

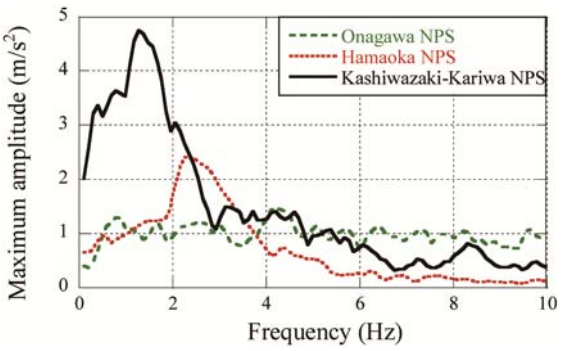

Fig.4 Comparison of maximum amplitude spectra

The specification of three seismic records is listed in Table 1. The profiles of shear-wave velocity in depth direction at three NPS sites are illustrated in Fig.3. The surface soil at the Kashiwazaki-Kariwa NPS and Hamaoka NPS is soft-rock with the shear-wave velocity smaller than 500m/s. On the other hand the soil of Onagawa NPS is

the hard rock with the shear-wave velocity larger than 1500m/s. The maximum amplitude spectra of three seismic records are compared in Fig.4. The maximum amplitude spectra of the seismic record at the Kashiwazaki-Kariwa NPS exceeded those of other records. The record 1R2 (EW) is compared with an artificial wave at the Kashiwazaki-Kariwa NPS by the non-stationary Fourier spectra (see Fig.5). The dominant components of the artificial wave scatter in the frequency and time domains with the amplitude of 2.0m/s^2. On the other hand the single dominant component is observed in 1R2(EW) and the amplitude exceed 4.0m/s^2, which is more than two times larger than the maximum amplitude of the artificial wave (see Fig.6). The pulse wave of 1R2(EW) is an extraordinary seismic event. In the previous research (Kamagata and Takewaki, 2013a), the authors focused on the pulse wave of 1R2(EW) and investigated the non-stationary property of the seismic records.

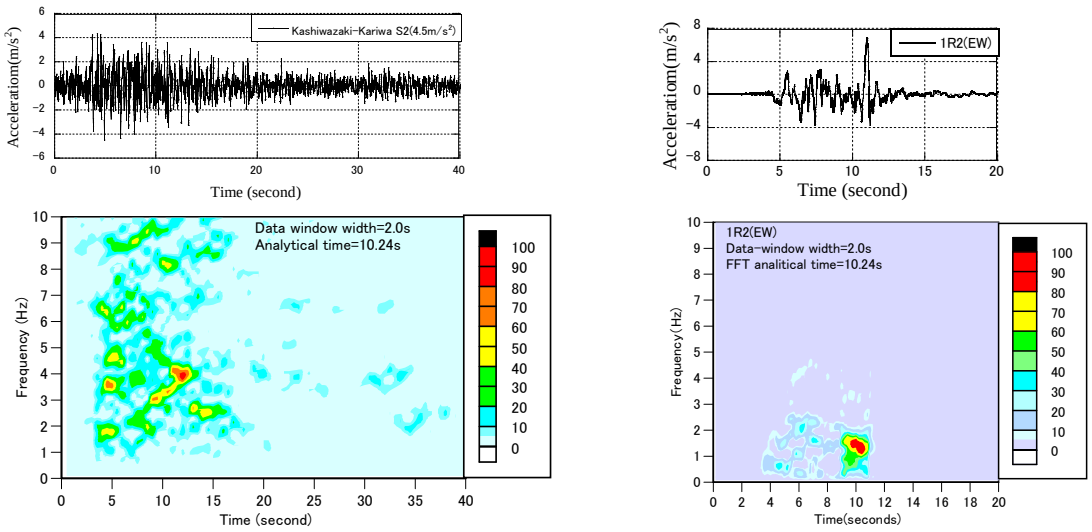

S2 design artificial wave　　1R2(EW) seismic record

Fig.5 Non-stationary Fourier spectra

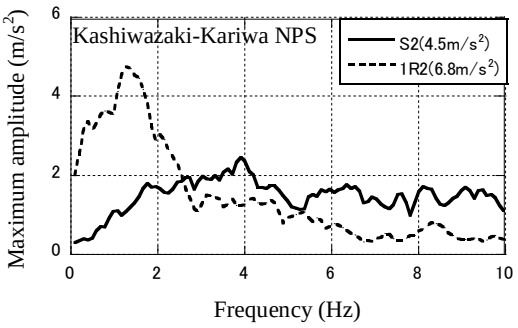

Fig.6 Maximum amplitude spectra

Different from the approach in Kamagata and Takewaki (2013a), the occurrence mechanism of large accelerations at the Kashiwazaki-Kariwa nuclear power station during the Niigata-ken Chuetsu-oki earthquake in 2007 is investigated in this paper by the analysis of a simplified numerical model. Regarding the soil-structure interaction (SSI) (Wolf 1985, 1988), many researches have been conducted without the consideration of non-linear interaction between an embedded building and its surrounding soil since the nuclear power station was constructed at the hard rock site. The recent seismic events exceeded the assumption of elastic design and the research of non-linear soil-structure interaction has been conducted (Bolisetti and Whittaker, 2011, Gazetas et al., 2013, Kishida and Takewaki 2010).

The numerically integrated displacement profile (red dotted line) is illustrated with the acceleration profile (blue solid line) in Fig.7, from which the authors have found the large acceleration related to the second deformation with the amplitude of 0.4m at 10s (Kamagata and Takewaki, 2013a).

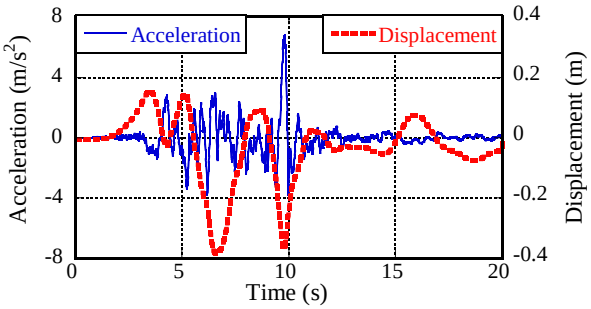

Fig.7 Acceleration and displacement profiles during Niigata-ken Chuetsu-oki earthquake in 2007

The displacement profiles of the EW component (blue solid line) which recorded the maximum acceleration 6.8m/s^2 and the UD component (dotted line) are illustrated with the orbit in Fig.8. Two cycles of displacement after 5s are discriminated by the colors of brown and green. Both amplitudes of peak to peak are almost 0.36m and the duration of second cycle is shorter than the first cycle. Both displacement profiles are illustrated as an orbit, in which the second cycle of displacement is found to be the horizontal movement with high speed since the interval of neighboring dots is wide.

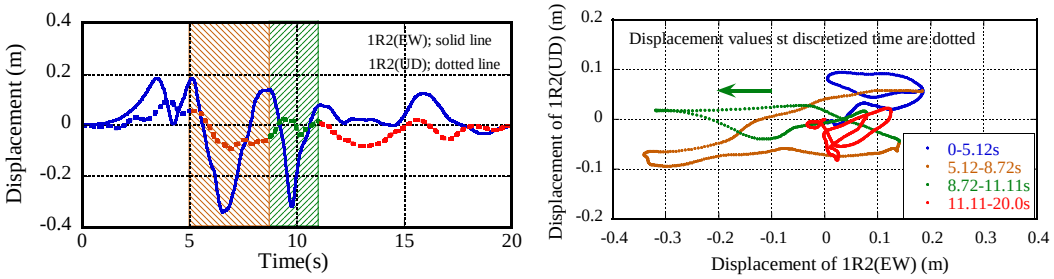

Fig.8 Displacement profile and orbit of EW and UD components of ground motion during Niigata-ken Chuetsu-oki earthquake in 2007

Regarding the occurrence mechanism of large amplitude acceleration, the third asperity was assumed near the Kashiwazaki-Kariwa NPS site and amplification by the fold structure 2km below the ground surface was estimated by Tokyo Electric Company (2007, 2008). The second author inspected the seismic hazard at the Kashiwazaki-Kariwa NPS after the earthquake in 2007 as a member of JNES and detected the less damage of the reactor building. He also investigated the non-linear interaction between the building and the side soil from the subduction of side soil at the reactor building and found that the maximum amplitude acceleration was caused by the pulse wave. The non-linear behavior in the side soil and the transient response process are new view-points in this paper. On the other hand, the previous research was based on the stationary linear response process as shown by Der Kiuregian (1996) and Wolf (1985, 1988).

Based on the field investigation the Tokyo Electric Power Company reported on the subduction at the side-soil of the embedded foundation and the residual deformation of foundation in the vertical direction (Tokyo Electric Power Corporation, 2007, 2008). The authors pointed out the importance of the research on the non-linear contact behavior between the embedded building and its surrounding soil and the rocking of the foundation as shown in Fig.9 (Kamagata and Takewaki, 2013a).

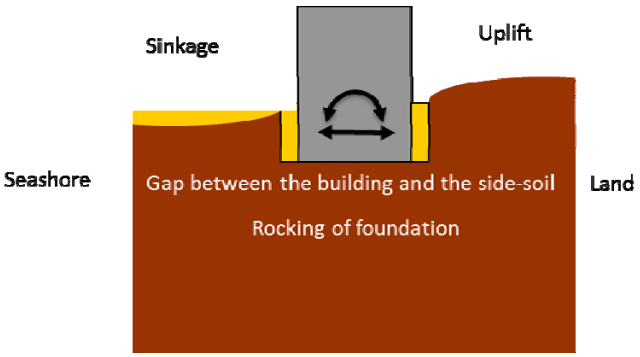

Fig.9 Non-linear contact behavior between embedded building and surrounding soil

There is an issue on the understanding of the maximum values of earthquake ground motions. Strasser and Bommer (2009a, b) discussed the possibility to predict the level of the maximum values of earthquake ground motions based on currently available observation and a statistical exercise involving the sampling of spatially correlated stochastic ground-motion fields (Der Kiureghian 1996). They also pointed out that some of the simplifying assumptions made regarding the treatment of uncertainties in conventional probabilistic seismic hazard analysis (PSHA) procedures may contribute to generate overly conservative results when extended to low annual frequencies of excess and there is a limit to discuss such issue only from a very short span of past observations. Castaños and Lomnitz (2010) commented on this issue and recommended the use of extreme-value statistics. In response to this comment, Strasser and Bommer (2010) pointed out that their intention is to warn against overly optimistic inference from very limited data. On this issue, Ben-Haim (2001, 2006) introduced a non-probabilistic concept called 'Info-gap theory' which uses only the interval of an uncertain parameter (not a probabilistic distribution). In the research field of structural engineering, the critical excitation was proposed by Drenick (1970). Takewaki (2006, 2013) formulated several critical excitation methods for important structures based on this concept. He pointed out that the acceleration power (time integration of squared ground acceleration) plays a key role rather than the maximum ground acceleration with large variability. In order to respond to such worst case, Kobori, Kanayama and Kamagata (1989) investigated the seismic response control considering the use of special structural devices with the nonlinear property.

2. Bi-linear restoring-force characteristic with gap-slip process

Different from the preliminary approach (Kamagata and Takewaki, 2013a) based on analysis of the seismic records, the subduction at the contacting-soil to the embedded building is investigated by a numerical analysis. A bi-linear restoring-force characteristic with a gap-slip process is adopted and the iteration method is introduced in the incremental numerical integration scheme.

2.1 Numerical integration using iteration for convergence

In the numerical integration, the trapezoidal rule is adopted with iteration to satisfy the equilibrium at each incremental step. Let $[M],[C],[K]$ denote the mass, damping and stiffness matrices and $\{\ddot{y}(t)\}$, $\{x(t)\}$ denote the ground acceleration and the response displacement. The equations of motion can be described by

$$[M]\{\ddot{x}(t)\}+[C]\{\dot{x}(t)\}+[K]\{x(t)\}+\{F_C{}^i(t)\}=-[M]\{\ddot{y}(t)\} \quad (1)$$

The restoring force vector $\{F_C{}^i(t)\}$ of the link springs in the *i*-th iteration step at time *t* can be expressed by

$$\{F_C{}^i(t)\} = \{f(x(t), x^i(t+\Delta t))\} \tag{2}$$

Eq.(2) means that the restoring force of the link spring with a non-linear restoring-force characteristic can be evaluated by the displacement $\{x(t)\}$ of the previous time step and the displacement $\{x^i(t+\Delta t)\}$ of the next time step (Δt is an incremental time in the analysis). The corresponding response acceleration may be expressed by

$$\{\ddot{x}^i(t+\Delta t)\} = [A]^{-1}\left[\{F_S(t+\Delta t)\} + \{F_R(t)\} + \{F_C{}^i(t+\Delta t)\}\right] \tag{3}$$

where

$$[A] = [M] + 0.5\Delta t[C] + 0.25\Delta t^2[K] \tag{4}$$

$$\{F_S(t+\Delta t)\} = [M]\{\ddot{y}(t+\Delta t)\} \tag{5}$$

$$\{F_R(t+\Delta t)\} = -[G_1]\{\ddot{x}(t)\} - [G_2]\{\dot{x}(t)\} - [G_3]\{x(t)\} \tag{6}$$

$$[G_1] = 0.5\Delta t[C] + 0.25\Delta t^2[K] \tag{7}$$

$$[G_2] = [C] + \Delta t[K] \tag{8}$$

$$[G_3] = [K] \tag{9}$$

$$\{F_C{}^0(t+\Delta t)\} = \{F_C(t)\} \tag{10}$$

$$\{\dot{x}^i(t+\Delta t)\} = \{\dot{x}(t)\} + 0.5\Delta t[\{\ddot{x}(t)\} + \{\ddot{x}^i(t+\Delta t)\}] \tag{11}$$

$$\{x^i(t+\Delta t)\} = \{x(t)\} + 0.5\Delta t\{\dot{x}(t)\} + 0.25\Delta t^2[\{\ddot{x}(t)\} + \{\ddot{x}^i(t+\Delta t)\}] \tag{12}$$

The equilibrium is satisfied by iteration for the following condition.

$$\{F_C{}^{i+1}(t)\} = \{f(x(t), x^{i+1}(t+\Delta t))\} \tag{13}$$

The corresponding response acceleration may be expressed by

$$\{\ddot{x}^{i+1}(t+\Delta t)\} = [A]^{-1}\left[\{F_S(t+\Delta t)\} + \{F_R(t)\} + \{F_C{}^{i+1}(t+\Delta t)\}\right] \tag{14}$$

The convergence of equilibrium is evaluated by Equations (12) and (13).

$$\varepsilon = \sum_{J=1}^{N}\left|\{\ddot{x}_J{}^{i+1}(t+\Delta t)\} - \{\ddot{x}^i{}_J(t+\Delta t)\}\right| \Big/ \sum_{J=1}^{N}\left|\{\ddot{x}_J{}^{i+1}(t+\Delta t)\}\right| \tag{15}$$

$$\varepsilon \le \varepsilon_{PV} \quad (\varepsilon_{PV}: \text{specified value}) \tag{16}$$

The accuracy of the iteration is discussed in Appendix-1.

2.2 Analytical model of non-linear soil-structure interaction

An assumed amplification mechanism in the acceleration response is verified by

using the 3DOF model as shown in Fig.10. The restoring-force characteristic of the link spring between the building foundation and its surrounding soil is modeled by the bi-linear gap-slip process as shown in Fig.11.

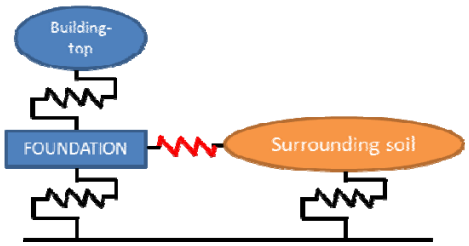

Fig.10 Analytical model of interaction between building and surrounding soil

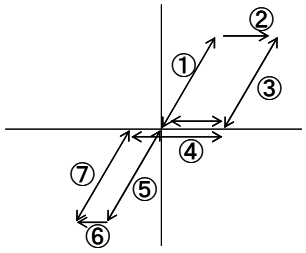

Fig 11 Restoring-force characteristic of link spring

Table 2 Parameter of analytical model

	Mass ($\times 10^7$kg)	Shear stiffness ($\times 10^7$N/mm)	Yielding stiffness ($\times 10^7$N/mm)	Elastic limit (mm)
Building-top	20.0	10.0	-	-
Building-foundation	20.0	10.0	-	-
Surrounding soil	100.0	100.0	-	-
Interaction spring	-	100.0	1.0	0.05

The model parameters are shown in Table 2. The natural periods without and with interaction between the building and its surrounding soil are shown in Table 3. The fundamental mode without interaction is the eigenmode of the building and the natural period is 0.459s (2.18Hz). The second mode without interaction is the eigenmode of the surrounding soil and the natural period is 0.201s (4.98Hz). The fundamental natural period of 0.318s (3.14Hz) with interaction is shorter than that without interaction due to the effect of the embedded foundation.

Table 3 Natural period without and with interaction

	First mode	Second mode	Third mode
$T_{f(}$ (s)	0.459	0.201	0.175
T_i (s)	0.318	0.194	0.076

(T_f: natural period without interaction, T_i: natural period with interaction)

3. Response to Ricker wavelet

The resemblance of the pulse wave of the seismic record and the Ricker wavelet as shown in Fig.12 has been pointed out (Kamagata and Takewaki, 2013a, Kamagata, 2009,

Japan Nuclear Energy Safety Organization, 2009b). In order to investigate the effect of the pulse wave on the seismic response in more detail, the Ricker wavelet is used in this section.

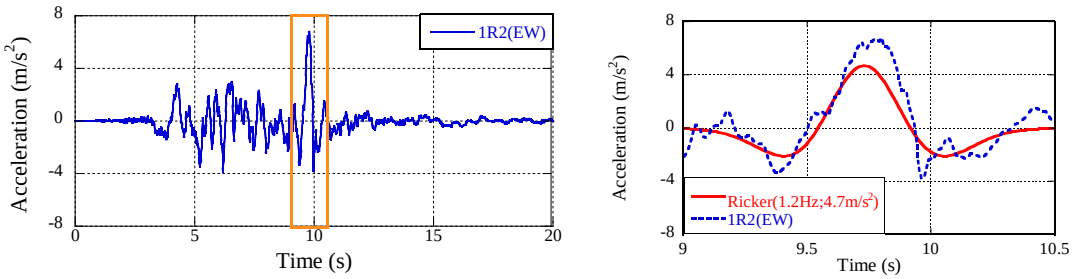

Fig.12 Identification of pulse wave by Ricker wavelet (right: magnified)

Analytical conditions are as follows.

(1) Input wave; Ricker wavelet (3Hz) of amplitude 0.2m/s^2

(2) Restoring-force characteristic; Bi-linear with gap-slip process

(3) Yielding stiffness Gy=0.01 × initial stiffness G

(4) Elastic limit deformation Dy=0.5mm

(5) Damping ratio=5%

The acceleration and displacement profiles are illustrated in Fig.13.

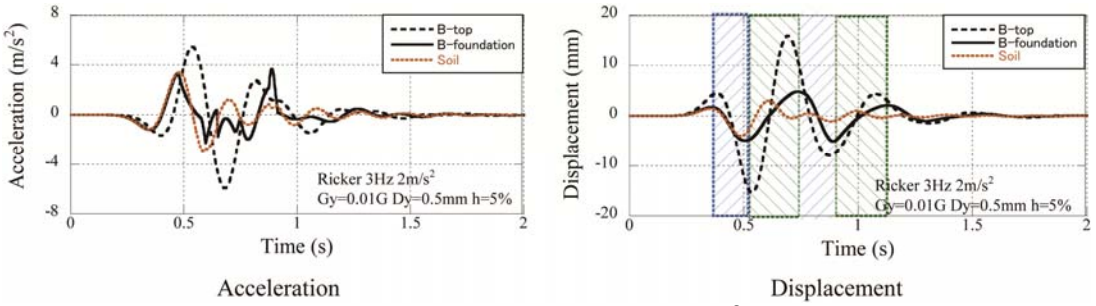

Fig.13 Acceleration and displacement response profiles by Ricker wavelet

The maximum acceleration of the foundation occurs after the main shock of the Ricker wavelet (0.88s). In the displacement profile of the foundation, the period differs in each half cycle (shaded by blue and green color) and the period of the surrounding soil (brown colored line) is shorter than that of the building, which is caused by the non-linear interaction between the foundation and its surrounding soil.

The force profile of the link-spring is illustrated with the acceleration profile in Fig.14. The maximum pulse in the acceleration profile occurs after the input of Ricker wavelet, which is coincident with the ends of the gap-slip process in the link-spring. The sharp change of the supporting force by the surrounding soil appears to cause the large pulse in the acceleration profile like a collision phenomenon.

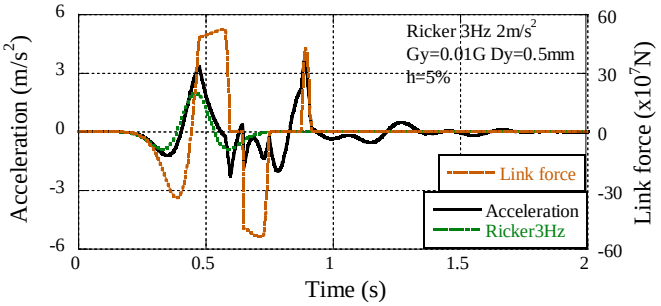

Fig.14 Relation of acceleration and link-force profiles

The hysteresis of the link-spring is illustrated in Fig.15, which shows a yielding process twice in the positive and the negative directions and the peak-to-peak amplitude is 9mm. The energy profiles (time histories) of three shear-springs and one link-spring are illustrated in Fig.16. The occurrence time of the maximum energy differs in each energy profile. The maximum absorbed energy of the link-spring reaches to 0.42Nm.

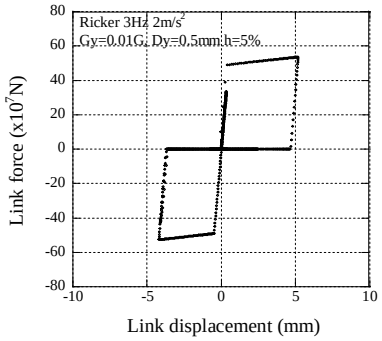

Fig.15 Hysteresis loop of link spring

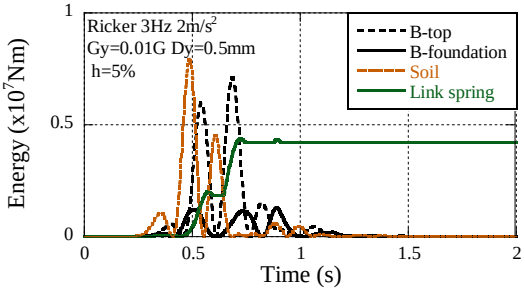

Fig.16 Energy profile

3.1 Influence of elastic limit in soil deformation

The influence of the elastic limit (D_y) in soil deformation on the seismic response is evaluated analytically. The following two cases are considered.

CASE-A1; D_y=0.5mm, G_y=0.01G

CASE-A2; D_y=1.0mm, G_y=0.01G

G_y is the post-yielding stiffness.

The acceleration and displacement profiles are illustrated in Fig.17. In the acceleration profile of CASE-A2, the maximum acceleration 4.63m/s^2 occurs in the free vibration process. In the displacement profiles, the phase of CASE-A1 delayed from that of CASE-A2 after 0.5s and the dual peaks are observed in CASE-A2.

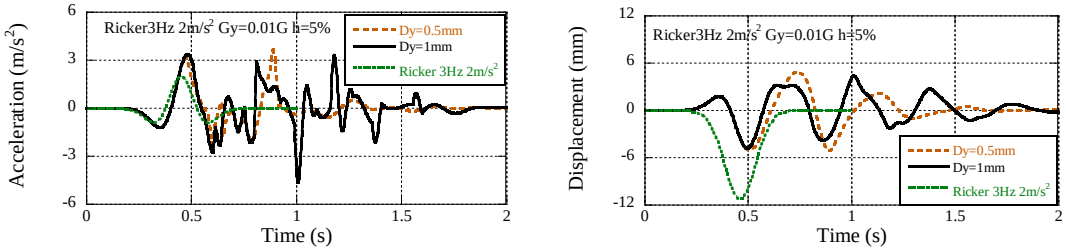

Fig.17 Acceleration and displacement response profiles by Ricker wavelet (3Hz)

The hysteresis curves of both cases are illustrated in Fig.18. The maximum amplitude of CASE-A1 (5.2mm) is 1.7 times of CASE-A2 (3.0mm). The created gap width of CASE-A1 (8.2mm) is 2.6 times of CASE-A2 (3.1mm). It can be said that the difference of the elastic limit gives a major influence on the seismic response.

The energy profiles (time histories) are illustrated in Fig.19. The energy of CASE-A1 (0.42Nm) is 1.35 times of CASE-A2 (0.31Nm).

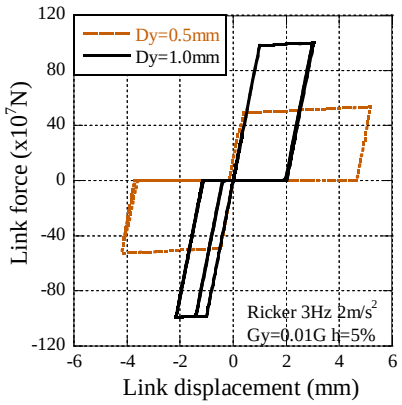

Fig.18 Comparison of hysteresis loops

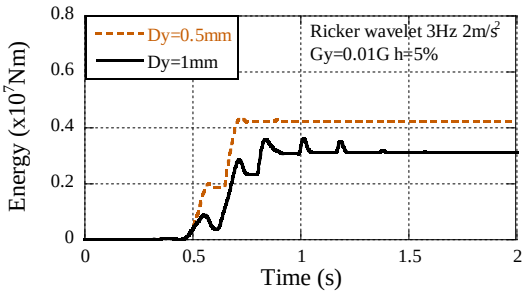

Fig.19 Comparison of energy profiles

3.2 Influence of soil post-yielding stiffness

The influence of the post-yielding stiffness (G_y) in soil deformation on the seismic response is evaluated analytically. The following two cases are considered.

1. CASE-B1; G_y=0.01G , D_y=0.5mm
2. CASE-B2; G_y=0.1G , D_y=0.5mm

The parameters of Ricker wavelet are frequency=3.0Hz and the amplitude=2.0m/s^2.

The acceleration and displacement profiles of CASE-B1 and CASE-B2 are illustrated with the Ricker wavelet in Fig.20. The maximum acceleration in the case of CASE-B2 is 30% larger than that of CASE-B1. The maximum displacements of both cases are almost the same. It can be said that the difference of the post-yielding stiffness gives less influence on the seismic response.

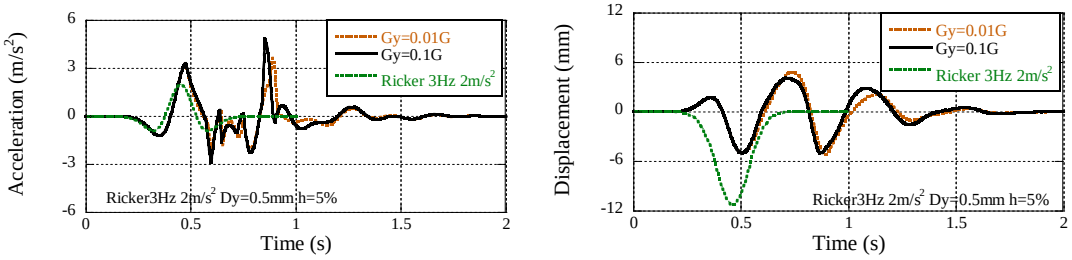

Fig.20 Acceleration and displacement response profiles of Ricker wavelet (3Hz)

Hysteresis curves in both cases are illustrated in Fig.21. The created gap width of CASE-B1 (8.2mm) is 1.3 times of CASE-B2 (6.3mm). The energy profiles (time histories) of the link-spring are compared in Fig.22. The energy profiles of the link-spring are coincident in both cases and the absorbed energy of the link-spring reached to 0.42Nm.

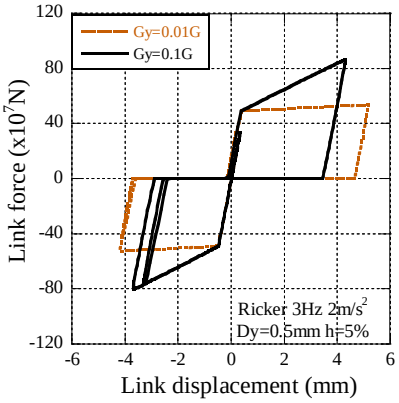

Fig.21 Comparison of hysteresis loops

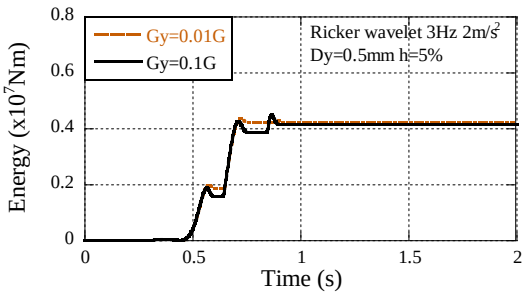

Fig.22 Comparison of energy profiles

3.3 Influence of input level

The restoring-force characteristics of the non-linear system lead to a non-proportional relation between the input level and the output level. As for the input wave, the Ricker wavelet of 3Hz is adopted and seven levels from 0.5m/s^2 to 2.0m/s^2 with a pitch of 0.5m/s^2 are analyzed. The acceleration and displacement profiles of the foundation are compared in Fig.23.

In the acceleration profiles, the maximum response is related to the pulse wave which occurs at a different time in each input level. In the level from 1.5m/s^2 to 2.0m/s^2, the maximum response occurs after the main part of the Ricker wavelet.

In the displacement profiles, the maximum response occurs in the second cycle. This resembles the occurrence mechanism of the large acceleration at the seismic record of the Kashiwazaki-Kariwa nuclear power station during the Niigata-ken Chuetsu-oki earthquake in 2007.

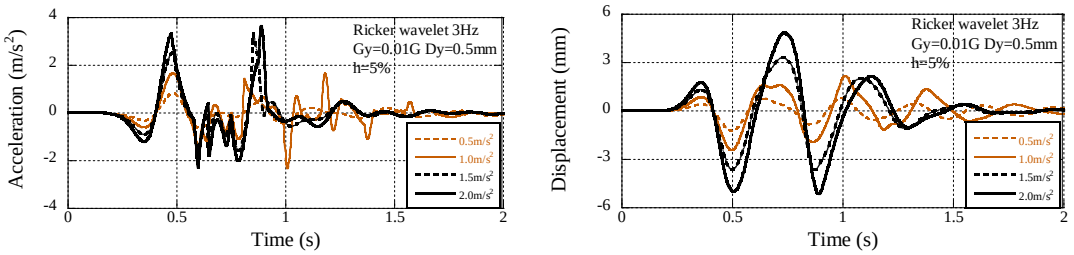

Acceleration response　　Displacement response

Fig.23 Comparison of acceleration and displacement response profiles (Dy=0. 5mm)

The linear model is analyzed for the link-spring in order to evaluate the amplification of the non-linear model. The maximum responses of the foundation are evaluated as the amplification ratio from that of the linear model (see Fig.24). The amplification ratio of the acceleration exceeds 1.2 at the input-level from 1.0m/s^2 to 1.75m/s^2. The amplification ratio of the foundation is not proportional to the input-level. The amplification ratio of the link-spring displacement is larger than 1.0 at the input-level larger than 0.5m/s^2 and the incremental amplification ratio is the largest at the input level from 0.75m/s^2 to 1.0m/s^2.

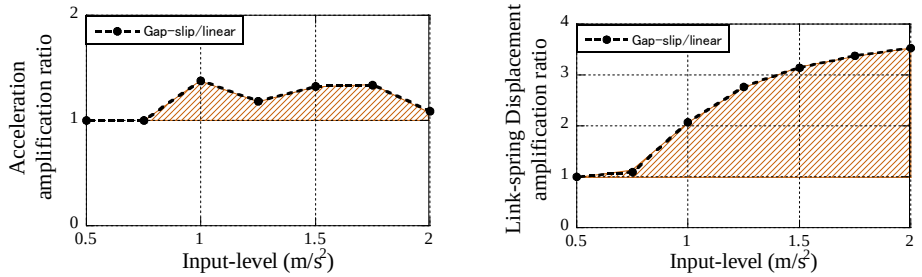

Acceleration　　Link-spring Displacement

Fig.24 Amplification ratio to linear model

The characteristic of the amplification ratio at the link-spring is caused by the phase of the foundation (black line) and the surrounding soil (brown line) (see Fig.25).

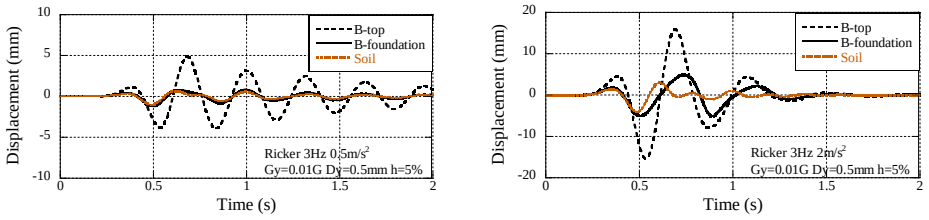

Input level 0.5 m/s^2　　Input level 2.0m/s^2

Fig.25 Comparison of displacement profiles at different heights

The dominant frequency components in the displacement profile of the foundation and the surrounding soil are analyzed by the non-stationary Fourier spectra as shown in Fig.26 (Trifunac, 1971, Kamagata, 1991). The dominant frequency component of the foundation is 2.5Hz with the amplitude of 3.5mm which is resonant to the main shock of the Ricker wavelet. The dominant frequency components of the surrounding soil scatter in the frequency from 3.0Hz to 5.0Hz with the amplitude of 1.2mm. The frequency 5Hz is coincident with the natural vibration frequency of the surrounding soil (see Fig.27).

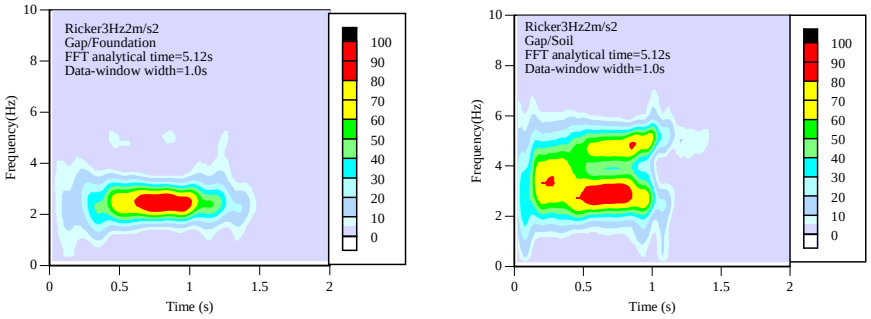

Foundation Soil

Fig.26 Non-stationary Fourier spectra of displacement profile

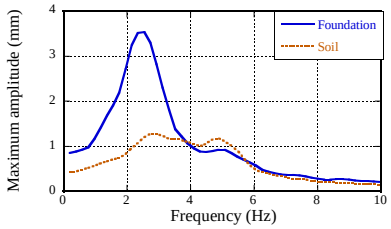

Fig. 27 Maximum amplitude spectra of displacement profile

The hysteresis of the link-spring is compared with the input-level of 1.0m/s^2 and 2.0m/s^2 in Fig.28 and the relation between the created gap-width and the input level is illustrated in Fig.29. The gap is created from the input level of 0.75m/s^2 and increases linearly with the increase of the input level.

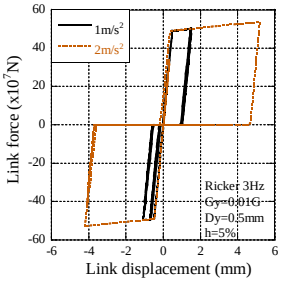

Fig.28 Comparison of hysteresis loops

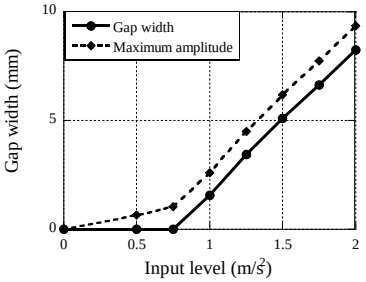

Fig.29 Gap width with respect to input level

Fig.30(a) shows the time histories of the absorbed energy by the link spring for four different input levels. Fig.30(b) indicates that the absorbed energy by the link-spring increases linearly with the increase of the input level larger than 0.75m/s^2.

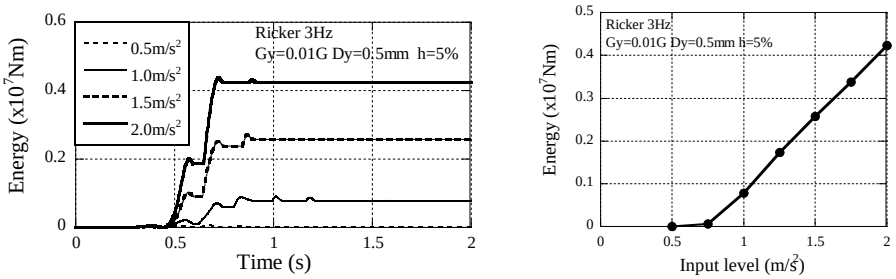

(a) (b)

Fig.30 Comparison of absorbed energy by link spring, (a) time histories, (b) variation with respect to input level

3.4 Influence of input frequency

Consider the fundamental and second natural frequencies of the analytical model. The Ricker wavelets are adopted at the frequency from 2Hz to 5Hz as shown in Fig.31.

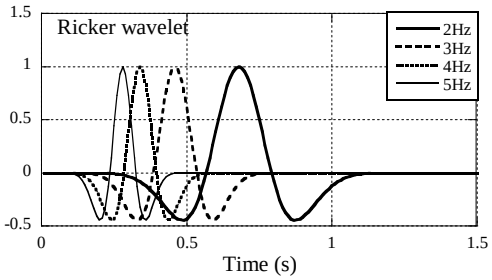

Fig.31 Ricker wavelet with frequency from 2Hz to 5Hz

The amplitude of the Ricker wavelet is set to 2.0m/s^2. The acceleration and displacement response profiles of the foundation are illustrated in Fig.32. The acceleration profiles of 3Hz and 4Hz have two peaks. One of which corresponds to the main shock of Ricker wavelet and the other is caused in the free vibration. The amplitude of the displacement profile becomes larger as the frequency becomes smaller.

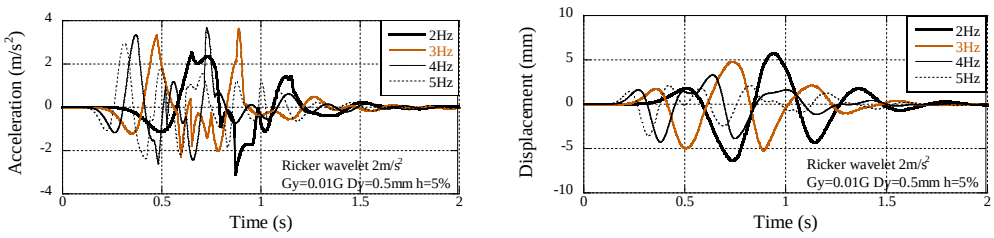

Acceleration profile Displacement profile

Fig.32 Comparison of input level（Dy=0.5mm）

As shown in Fig.33, the pulse wave in the acceleration profile is related to the pulse of the link-force profile. In the case of 2Hz, no pulse-like wave is observed after the input. On the other hand, a pulse-like wave is observed in the case of 3Hz, which causes the maximum acceleration.

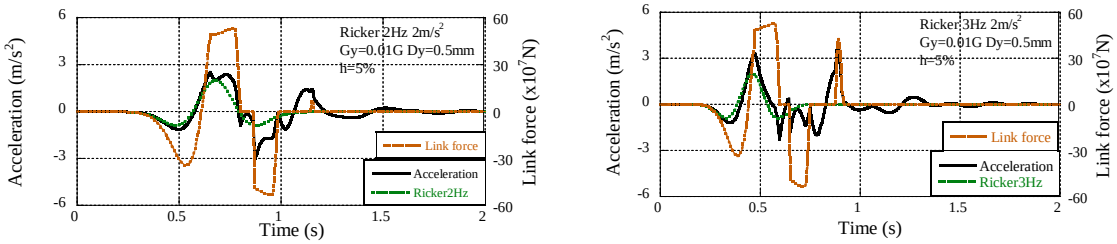

Ricker 2Hz Ricker 3Hz

Fig.33 Acceleration profile and link force profile

The dominant frequency components of the acceleration profiles are analyzed by the non-stationary Fourier spectra as shown in Fig.34. The dominant frequency components are different in each central frequency of the Ricker wavelet. In the case of 2Hz, the dominant frequency component appears in the duration from 0.5s to 1.0s. In the case of 3Hz, peculiar dominant components appear and the main dominant component at 3Hz appears at 0.3s. This may be related to the central frequency of the Ricker wavelet and this shifts to a lower frequency toward to 0.4s. It continues from 0.4s to 1.0s and the additional dominant component of 5Hz appears from 0.5s to 1.0s.

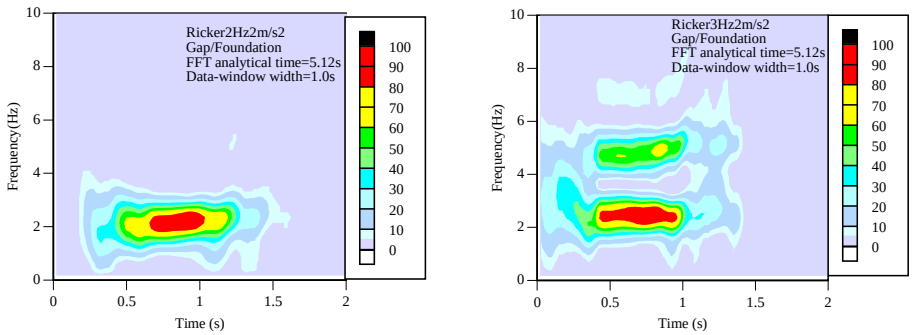

Ricker 2Hz Ricker 3Hz

Fig.34 Non-stationary Fourier spectra of acceleration profile

In the case of 2Hz the main dominant frequency component is 2.1Hz with the amplitude of 1.51m/s^2 and in the case of 3Hz the main dominant frequency component is 2.5Hz with the amplitude of 1.15m/s^2. The additional dominant frequency component appears at 4.9Hz with the amplitude 0.97 m/s^2 (see Fig.35). A higher

frequency component occurs after the input, which is induced in the free vibration in the gap-slip process.

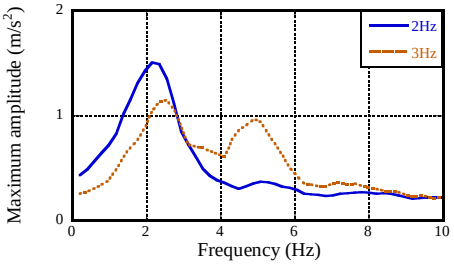

Fig.35 Maximum amplitude spectra

The maximum acceleration at the foundation and the maximum deformation of the link-spring are compared in Fig.36. The maximum acceleration at 3.5Hz and the maximum deformation of the link-spring at 2.5Hz are the largest in the frequency from 2.0Hz to 5.0Hz, which may result from the resonance at the fundamental natural frequency (3.14Hz).

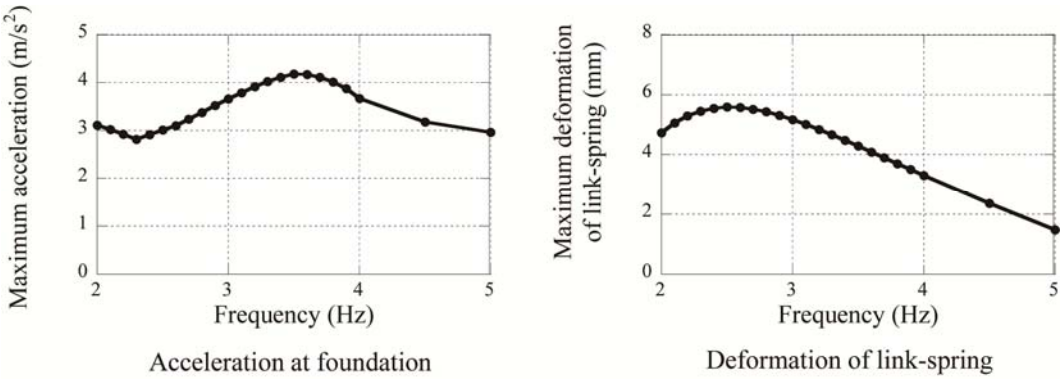

Fig.36 Comparison of maximum response values

4. Response to continuously sweeping sinusoidal wave

In order to investigate the influence of the input wave frequency, the following continuously sweeping sinusoidal waves as shown in Fig.37 are adopted.

$$\text{Sweep-A}\quad \ddot{y}(t)=\sin\left\{2\pi\left(1+\alpha\frac{t}{T_N}\right)t\right\}\ ;\ \alpha=8.0,\ T_N=10.0\text{s} \tag{17}$$

$$\text{Sweep-B}\quad \ddot{y}(t)=\sin\left\{2\pi\left(9-\alpha\frac{t}{T_N}\right)t\right\}\ ;\ \alpha=8.0,\ T_N=10.0\text{s} \tag{18}$$

where T_N is the duration.

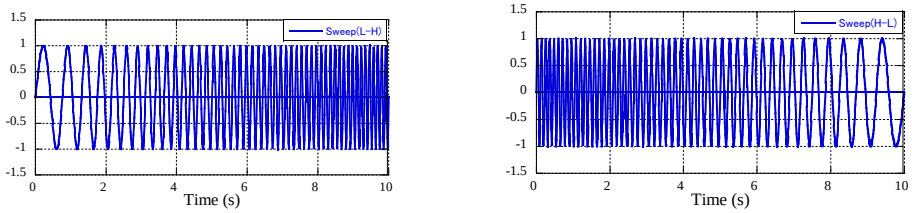

Sweep-A Sweep-B

Fig.37 Sinusoidal wave with phase modulation

They are analyzed by the non-stationary Fourier spectra. The dominant frequency components of both continuously sweeping waves change continuously in the duration (see Fig.38). The amplitude of the dominant component is 1.0m/s^2 and the property of input waves is analyzed (see Fig.39).

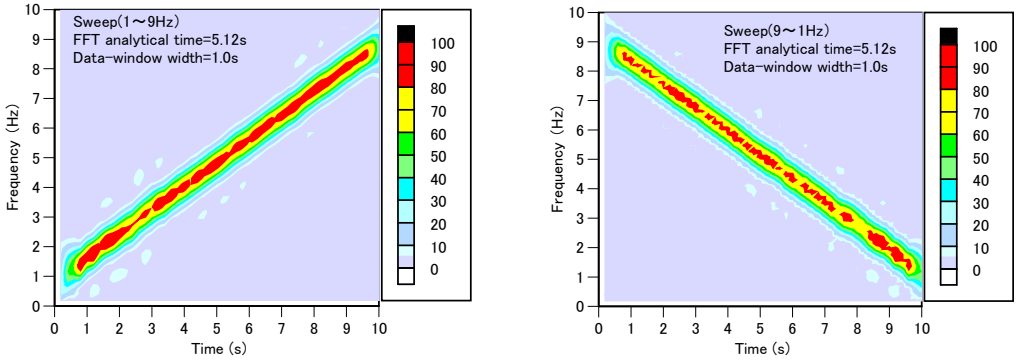

Sweep-A Sweep-B

Fig.38 Non-stationary Fourier spectra

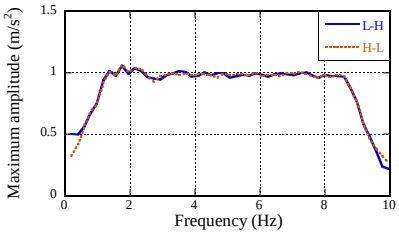

Fig.39 Maximum amplitude spectra

The response profiles by the continuously sweeping sinusoidal wave with the amplitude of 1.0m/s^2 are illustrated in Fig.40. In the acceleration profile, two kinds of resonant vibration occur, which are related to the fundamental and second natural modes of the model.

In the displacement profile, two kinds of resonant vibration occur at the foundation and continuously increasing amplification occurs at the building top. In addition, the

short resonant vibration from 4s to 6s occurs at the surrounding soil.

The response properties at the building top, the foundation and the surrounding soil are investigated on the influence of two kinds of continuously sweeping sinusoidal wave, which are denoted as sweep-A (form low to high frequency) and sweep-B (from high to low frequency).

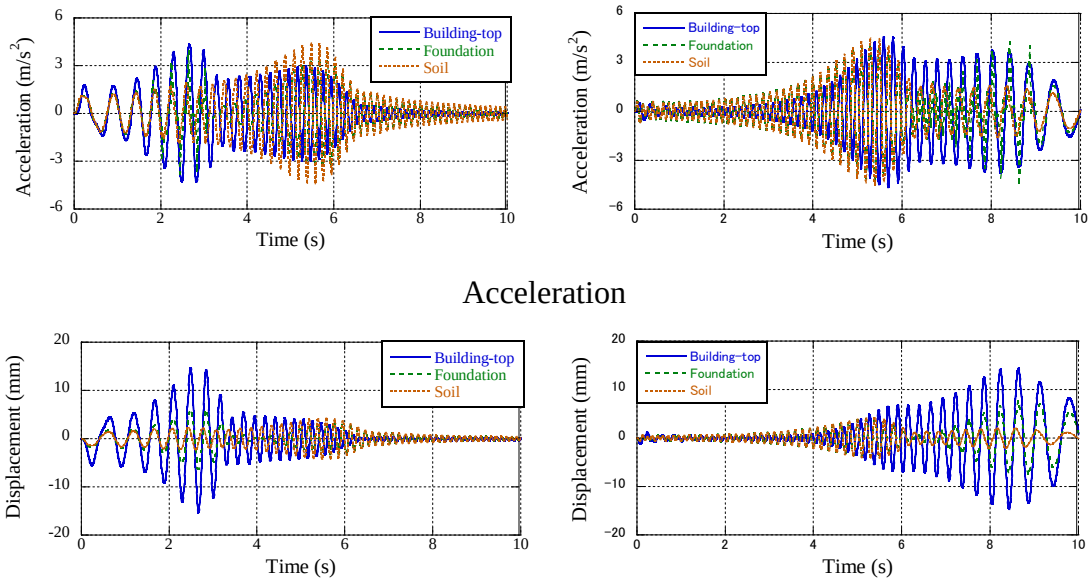

Acceleration

Displacement

Sweep-A Sweep-B

Fig.40 Comparison of response profiles

The acceleration and displacement profiles of the foundation in cases of sweep-A and sweep-B are compared in Fig.41. The pulse-like waves occur from 2 to 4s in the response of sweep-A and from 8 to 9s in the response of sweep-B with the amplitude of 4.0m/s^2. In the displacement profiles, two kinds of resonant vibration occur in both cases.

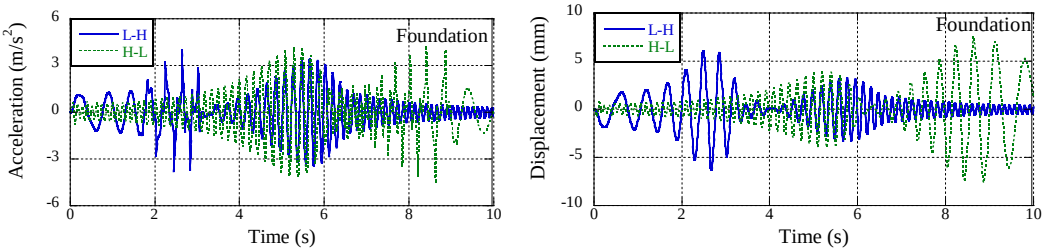

Acceleration Displacement

Fig.41 Comparison of response profile at building foundation

The non-stationary Fourier spectra of the acceleration profiles are illustrated in Fig.42. The dominant component occurs from 5s to 6s in both cases and the component of pulse-like wave occurs at 2Hz to 3Hz. The maximum amplitude in case of sweep-A occurs at 5.3Hz with the amplitude of 3.1m/s^2 and that in case of sweep-B occurs at 5.1Hz with the amplitude of 3.9m/s^2.

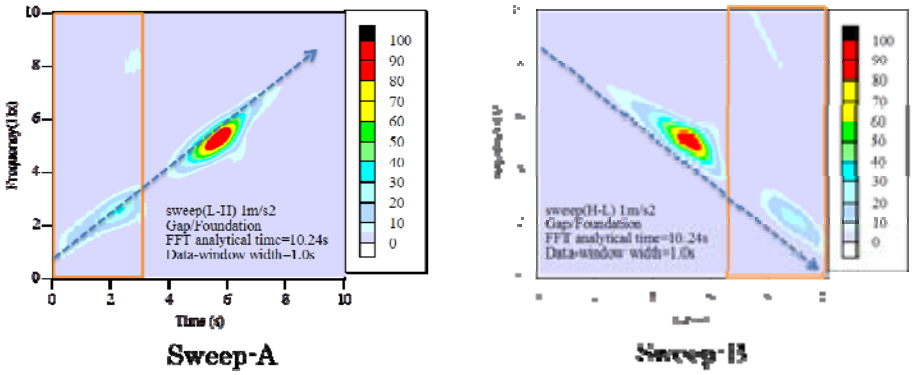

Sweep-A Sweep-B

Fig.42 Non-stationary Fourier spectra of acceleration profile

In order to investigate the pulse-like wave in detail (enclosed by orange colored line), the frequency range of the non-stationary Fourier spectra is expanded to 15Hz. In case of sweep-A, the dominant component of 8Hz occurs at around 3s and the subsequent dominant component from 10Hz to 8Hz occurs at 7 to 9s in case of sweep-B (see Fig.43). The amplitude at 8Hz is 1.0m/s^2 and the difference is small in both cases (see Fig.44).

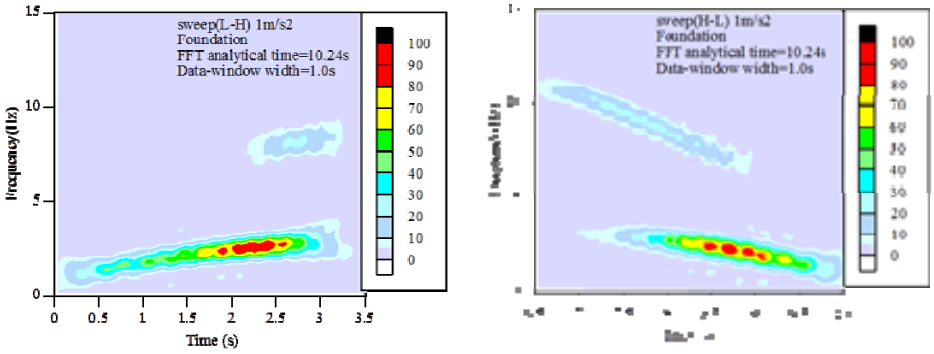

Sweep-A Sweep-B

Fig.43 High frequency components at foundation

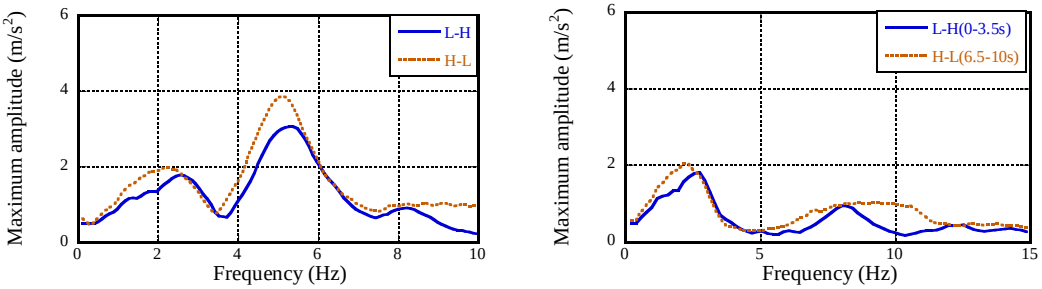

Duration of 10 second　　Duration of 3.5 second

Fig.44 Non-stationary Fourier spectra of acceleration profile at building foundation

The difference of the duration at higher frequency is related to the number of collapses in the gap-slip process, which is confirmed in the hysteresis curve of the link-spring as shown in Fig.45. The number of collapses is 4 in case of sweep-A and more than 10 in case of sweep-B. The subsequent enlargement of the gap leads to the change of frequency from 10Hz to 8Hz in case of sweep-B.

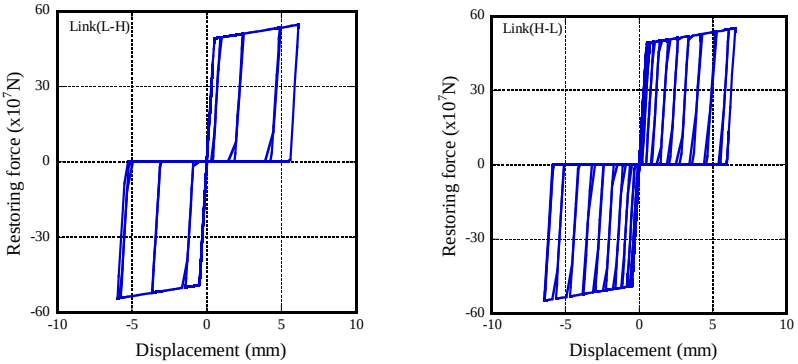

Sweep-A　　Sweep-B

Fig.45 Comparison of hysteresis loops

The energy profiles of the shear spring and the link-spring are illustrated in Fig.45. The magnitude of energy is related to the stiffnss and the response amplitude. The accumulated energy in the link-spring can be regarded as the plastic energy in the side soil of the embedded building (see Fig.46).

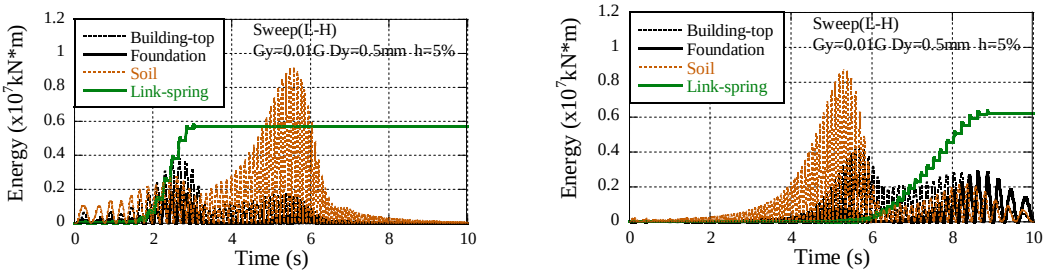

Sweep-A Sweep-B

Fig.46 Energy profile of shear spring and link spring

5. Conclusion

The mechanism of the large amplitude acceleration in the seismic record has been simulated by using a simplified 3DOF model in which the bi-linear restoring-force characteristic with a gap-slip process is adopted for the link-spring between the foundation and its surrounding soil.

In the simulation, the pulse-like wave occurs at the end of the gap-slip process which is similar to a collision behavior. The maximum acceleration occurs in the second cycle of large deformation, which is coincident with the behavior of the foundation of the reactor building at the Kashiwazaki-Kariwa nuclear power station during the Niigata-ken Chuetsu-oki earthquake in 2007. In the wide range of parameters, it has been found that the elastic limit displacement of soil has a major influence on the gap width of the foundation and its surrounding soil. The gap width became larger linearly as the input level increases.

Regarding the amplification behavior due to the deterioration of the side soil, the continuously sweeping sinusoidal wave has been adopted as the input wave. The dominant frequency components have been analyzed by the non-stationary Fourier spectra. It has been found that the deterioration of the side soil causes the shift of natural frequency to lower. This causes the amplification in the response to the continuously sweeping sinusoidal waves in high to low frequency. Moreover it has been observed that the cyclic enlargement of the gap width leads to the frequency shift of the higher mode by the collision at the end of the gap-slip process.

The occurrence mechanism of the large amplitude acceleration is not necessarily related to the asperity of the seismic faults and the research of the interaction between the building and its surrounding soil should be investigated by considering the nonlinear behavior. The nonlinear interaction between the embedded building and its surrounding soil may be one of the important factors in the large amplitude acceleration events. The maximum level of ground accelerations should be discussed in more detail from the viewpoints including various uncertainties (Strasser and Bommer 2009a, 2009b, 2010,

Castaños and Lomnitz 2010). Some of the simplifying assumptions made regarding the treatment of uncertainties in conventional probabilistic seismic hazard analysis (PSHA) procedures may contribute to generate overly conservative results when extended to low annual frequencies of excess and there is a limit to discuss such issue only from a very short span of past observations.

Acknowledgements

The authors are grateful to Tokyo Electric Power Corporation for providing the field investigation report and the seismic records of the Kashiwazaki-Kariwa nuclear power station during the Niigata-ken Chuetsu-oki earthquake in 2007 which were useful in evaluating the interaction between the building and its surrounding soil.

References

Ben-Haim, Y. 2001. “Information-gap decision theory: Decisions under severe uncertainty”, Academic Press, London.

Ben-Haim, Y. 2006. “Information-gap decision theory: Decisions under severe uncertainty”, Elsevier, Second edition, Oxford.

Bolisetti, C, Whittaker, AS. 2011. “Seismic structure–soil–structure interaction in nuclear power plant structures”. *Transactions, SMiRT 21*, 6–11, November, 2011, NewDelhi, India.

Castaños, H and Lomnitz, C. 2010. “Comment on “Review: Strong Ground Motions—Have We Seen the Worst?” by Fleur O. Strasser and Julian J. Bommer”, *Bulletin of the Seismological Society of America*, 100(4), 1836–1837.

Der Kiureghian, A 1996. “A coherency model for spatially varying ground motions”, *Earthquake Engineering Structural Dynamics*, 25; 99- 111.

Drenick, RF (1970),”Model-free design of aseismic structures”, *J. Engrg. Mech. Div.*, ASCE, **96**(EM4), 483-493.

Gazetas, G, Anastasopoulos, I, Adamidis, O, Kontoroupi, T. 2013. “Nonlinear rocking stiffness of foundations”. *Soil Dynamics and Earthquake Engineering*; 47: 83–91.

Japan Nuclear Energy Safety Organization, 2008, “Analysis of seismic motion occurred at Kashiwazaki-Kariwa nuclear power station in the Niigata-ken Chuetsu-oki earthquake 2007”, *Investigation Advisory Board of Seismic Safety*, (http://www.meti.go.jp/committee/materials/ download files/g80522a23j.pdf).

Japan Nuclear Energy Safety Organization, 2009a. “*Analysis of seismic records to evaluate the interaction between the building and the surrounding soil*”, JNES/SSD09-004 (in Japanese), (http://www.jnes.go.jp/content/000016346.pdf).

Japan Nuclear Energy Safety Organization, 2009b. “Analysis of seismic behavior of

building foundation by seismic records" JNES/SSD09-004 March 2009 (in Japanese), (Available from <http://www.jnes.go.jp/content/000016346.pdf> {Accessed on January 30th 2013}).

Kamagata, S. 1991. "Non-stationary spectra for seismic response control", *News & Topics Research & Development Structural Engineering (KRCEE0019111501)*, Kobori Research Complex (in Japanese).

Kamagata, S. 2009. "Non-stationary property of Niigata-ken Chuetsu-oki Earthquake on Kashiwazaki-Kariwa nuclear power plants (Occurrence mechanism of pulse-like wave)", *Annual meeting of Architectural Institute of Japan*, 1007-1008 (in Japanese).

Kamagata, S. Takewaki, I, 2013a. "Occurrence mechanism of recent large earthquake ground motion at nuclear power plant sites in Japan under soil-structure interaction", *Earthquakes and Structures*, 4(5), 557-585.

Kamagata, S. and Takewaki, I. 2013b. "New insights into seismic behavior of building and surrounding soil at Hamaoka nuclear power station during Suruga Bay earthquake in 2009", *Soil Dynamics and Earthquake Engineering*; 53: 73–91.

Kamagata, S. and Takewaki, I. 2013c. "Role of records during the 2011 off the Pacific coast of Tohoku earthquake in seismic resistant design of nuclear power station", *International Journal of Earthquake Engineering and Hazard Mitigation (IREHM)*, Vol. 1, No.1.

Kishida, A and Takewaki, I, 2010. "Response spectrum method for kinematic soil-pile interaction analysis", *Advances in Structural Engineering*, 13(1); 181-197.

Kobori, T, Kanayama, H. and Kamagata, S. (1989), "Active seismic response control systems for nuclear power plant equipment facilities", *Nuclear Engineering and Design*, 111, 351-356.

Nuclear Safety Commission of Japan, 2012. "Guideline of seismic design for nuclear power reactor facilities (revised version, draft)", March 14, (in Japanese) (http://www.nsc.go.jp/ senmon/shidai/genkishi/genkishi020/siryo2.pdf).

Strasser, FO and Bommer, JJ, 2009a. "Review: Strong ground motions—Have we seen the worst?", *Bulletin of the Seismological Society of America*, 99(5); 2613–2637.

Strasser, FO and Bommer, JJ, 2009b. "Review: Large-amplitude ground-motion recordings and their interpretations", *Soil Dynamics and Earthquake Engineering*, 29; 1305–1329.

Strasser, FO and Bommer, JJ, 2010. "Reply to "Comment on 'Review: Strong ground motions—Have we seen the worst?' by Fleur O. Strasser and Julian J. Bommer" ", *Bulletin of the Seismological Society of America*, 100(4), 1838–1839.

Takewaki, I. 2006. ''Critical excitation methods in earthquake engineering", Elsevier,

Amsterdam.

Takewaki, I. 2013. ‘‘Critical excitation methods in earthquake engineering”, Elsevier, Second edition, Amsterdam.

Tokyo Electric Power Corporation, 2007. “First report on the analysis of seismic records measured at Kashiwazaki-Kariwa nuclear power station on the Niigata-ken Chuetsu-oki earthquake 2007”, *press-release* July 20th 2007 (in Japanese), (http://www.tepco.co.jp/cc/press/ betu07_j/images/070730d.pdf)

Tokyo Electric Power Corporation, 2008. ‘‘Research on the seismic safety of the Kashiwazaki- Kariwa nuclear power station for the Niigata-ken Chuetsu-oki earthquake in 2007’’, *Investigation Advisory Board of Seismic Safety*, February 26th, 2008, (http://www.meti.go.jp/ committee/materials/downloadfiles/g80215b03j.pdf)

Trifunac, M.D. 1971. ‘‘Response envelope spectrum and interpretation of strong earthquake ground motion’’, *Bulletin of Seismological Society of America*, 61(2) 342-356.

Wolf, JP 1985. ‘‘Dynamic soil-structure interaction”, Prentice-Hall, Englewood Cliffs, New. Jersey.

Wolf, JP 1988. ‘‘Soil-structure-interaction analysis in time domain”, Prentice-Hall, Englewood Cliffs, New. Jersey.

Appendix-1 Influence of incremental time in numerical analysis

In the numerical integration, the time increment affects the accuracy of results. Using the 3DOF model, the analytical results for four time increments, such as 0.01s, 0.005s, 0.0025s and 0.00125s, are compared. The phase for 0.00125s is ahead of that for 0.01s. The difference ratio is evaluated and shown in Eq.(A-1). The relation of the difference ratio and the time increment is illustrated in Fig.A1-4 for the maximum acceleration and displacement. The difference ratio decreases linearly in the logarithmic axis. The difference ratio between 0.005s and 0.0025s is around 0.1% for the maximum acceleration value.

$$\varepsilon(\Delta t_{i+1}) = \left| V_{MAX}(\Delta t_i) - V_{MAX}(\Delta t_{i+1}) \right| / V_{MAX}(\Delta t_{i+1}) \qquad \text{(A1-1)}$$

$V_{MAX}(\Delta t_i)$: maximum value of a B-top response with Δt_i

$\Delta t_1 = 0.01, \Delta t_2 = 0.005, \Delta t_3 = 0.0025, \Delta t_4 = 0.00125$

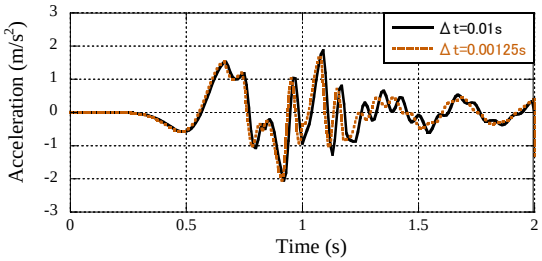

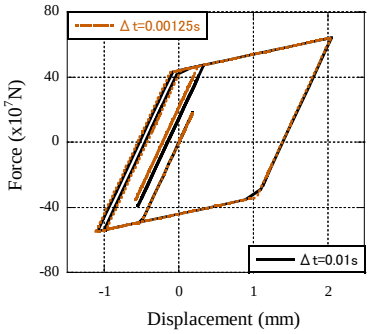

Comparison of acceleration profile　　Comparison of hysteresis loops

Fig.A1-1 Comparison of analytical results

Table-A1-1　Comparison of maximum response values

	Acceleration (gal)				Displacement (cm)			
	0.01s	0.005s	0.0025s	0.00125s	0.01s	0.005s	0.0025s	0.00125s
B-top	345.960	342.448	342.022	341.842	0.9573	0.9529	0.9522	0.9521
B-foundation	204.667	205.000	204.972	204.231	0.2942	0.2951	0.2952	0.2953
Soil	145.032	144.604	144.626	144.600	0.1986	0.1983	0.1982	0.1982
Diff. ratio	-	0.0103	0.0012	0.0005	-	0.0046	0.0007	0.0001

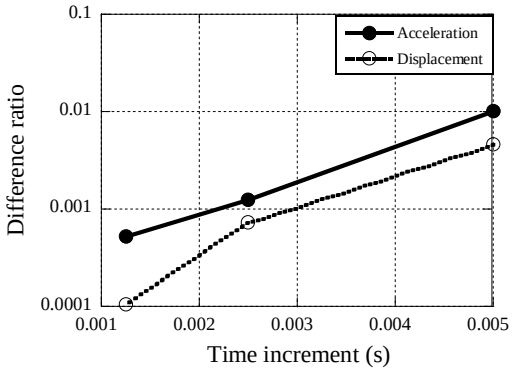

Fig.A1-2 Difference ratio and time increment

Appendix-2　Ricker wavelet

The Ricker wavelet is defined by Eq. (A2-1).

$$f(t)=\frac{\pi}{2}(\alpha-0.5)e^{-\alpha} \tag{A2-1}$$

$$\alpha=\left[\pi(t-t_S)\,f_P\right]^2 \tag{A2-2}$$

f_P ：central frequency

t_S ：occurrence time of maximum amplitude

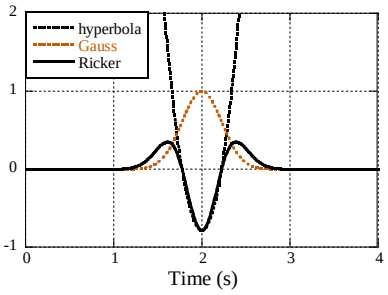

Fig.A2-1 Ricker wavelet

In Fig.A2-1, Eq. (A2-1) is subdivided into the hyperbolic function $\frac{\pi}{2}(\alpha - 0.5)$ and the Gauss function $e^{-\alpha}$. When the amplitude of the Ricker wavelet is the same as the acceleration profile, the displacement amplitude is decreased for the higher frequency as shown in Figs.A2-2 and A2-3.

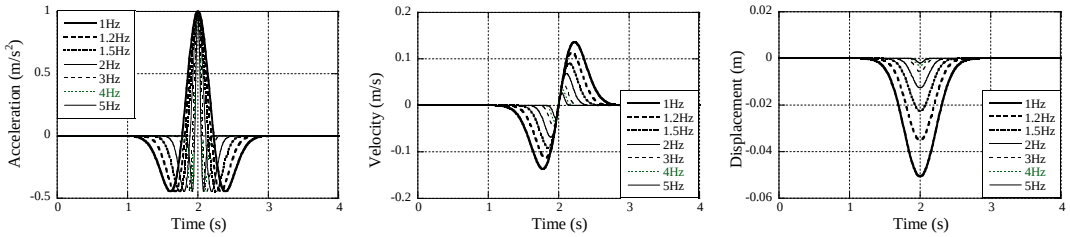

Fig.A2-2 Acceleration, velocity and displacement profiles

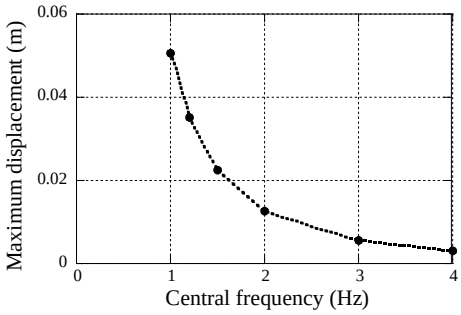

Fig.A2-3 Relation of central frequency and maximum displacement